Structural, electronic and optical characterization of bulk platinum nitrides: a first-principles study

Mohammed S. H. Suleiman[1, 2, *] and Daniel P. Joubert[1, †]

[1] *School of Physics, University of the Witwatersrand, Johannesburg, South Africa.*
[2] *Department of Physics, Sudan University of Science and Technology, Khartoum, Sudan.*

(Dated: January 24, 2013)

We present a detailed quantum mechanical non empirical DFT investigation of the energy-optimized geometries, phase stabilities and electronic properties of bulk Pt_3N, PtN and PtN_2 in a set of twenty different crystal structures. Structural preferences for these three stoichiometries were analyzed and equilibrium structural parameters were determined. We carefully investigated the band-structure and density of states of the relatively most stable phases. Further, GW_0 calculations within the random-phase approximation (RPA) to the dielectric tensor were carried out to derive their frequency-dependent optical constants of the most likely candidates for the true crystal structure. Obtained results were comprehensively compared to previous calculations and to experimental data.

CONTENTS

I. INTRODUCTION

Platinum is known to form simple binary compounds with other elements (e.g. PtF_4, PtI_2, PtO and PtS)[1]. However, platinum had not been known to form crystalline solid nitride, but other forms of platinum nitrides (e.g. PtN[1,2], PtN_2[1], $(PtN)_2$[1,2] and Pt_2N[2]) had been observed.

In January 2004, Soto[3] reported the preparation of platinum thin films containing up to $\sim$ 14 at. % nitrogen. The study concluded that platinum can form an incipient nitride phase with composition near to Pt_6N. Few months later, in May 2004, Gregoryanz and co-workers[1] published the discovery and characterization of solid crystalline platinum mono-nitride for the first time. The synthesis was carried out above 45 GPa and 2000 K but with complete recovery of the product at room pressure and temperature. The produced samples have a very high bulk modulus leading to important implications in high-pressure physics and technology. The 1:1 stoichiometry was assigned to the new nitride, and according to their XRD measurements, Gregoryanz et al. proposed three structures: B1, B3 and B17 (for description of the structures see sub-section II A below), all based on the Pt fcc sub-lattice. Due to some considerations, B1 and B17 were ruled out and B3 was assigned to the new product.

In addition to the well-crystallized and highly ordered regions, a common feature in the synthesized platinum nitrides is the presence of sub- or/and super-stoichiometric phases containing N or Pt vacancies and residual non-stoichiometric material distributed throughout the samples[1,4].

The work of Gregoryanz et al.[1] has stimulated many further theoretical studies[5–7] as expected by Gregoryanz and co-workers[1] themselves. However, theoretical work showed that PtN(B3) is elastically and thermodynamically unstable (see sub-section III A below). Accordingly, claiming that large errors are generally inevitable in the used experimental characterization methods[6,8], and due to other paradoxical facts[9] in the original experiment by Gregoryanz et al.[1], theoreticians questioned the chemical stoichiometry and the crystal structure of this new material and started to investigate other possibilities[8–10]. Moreover, the experimentally reported[1] high bulk modulus of the platinum nitride has not been reproduced by any reliable calculations and its mechanism is still an unclear open problem[5,9,10].

These investigations led to a kind of consensus that the compound does not crystallize in the proposed PtN(B3) phase[4], but the true stoichiometry and the true crystal structure have become now a matter of debate[6,9].

In an apparent attempt to respond to this debate, Crowhurst et al.[4] managed, in 2006, to to reproduce and characterize platinum nitride. Combining theory with

their own observed Raman spectrum, they came up with a conclusion to propose PtN_2(C2) and rejected PtN(B3), proposed by the first platinum nitride synthesizers[1], and PtN_2(C1), proposed in some theoretical works. Like the first proposed structures[1], C1[8] and C2[4] structures have the fcc sub-lattice of the metal.

Despite the considerable number of the subsequent theoretical studies, the discrepancy between theory and experiment in the structural and the physical properties of this nitride is not yet satisfactorily understood. Nevertheless, many transition metals can form more than one nitride[11]. Thus, it is of interest to know if platinum can form nitrides with different stoichiometries and/or crystal structures other than those proposed by the first platinum nitride synthesizers and other researchers.

In the present work, we present a comprehensive first-principles calculations of the equation of state, possible pressure-induced phase transitions, electronic and optical properties of crystalline Pt_3N, PtN and PtN_2 in a total of twenty different -previously proposed and new hypothetical- structural modifications. The work partly aims to solve some of the reported discrepancies. In addition, to the best of our knowledge, there is no available experimental or theoretical optical data for the platinum nitride, and the present study may be the first one to calculate the optical spectra of platinum nitrides.

II. CALCULATION METHODS

A. Stoichiometries and Crystal Structures

The structure and stability of solids are influenced by their chemical stoichiometry[12] and the electronic structure of the outer shells of atoms is a controlling factor in proposing any crystal structure[13]. Like other theoretical works (cf. Table I) we postulated various structure types that are not based on the observed fcc Pt sub-lattice. Our assignment of the following different chemical stoichiometries and crystal structures is based on the fact that many transition-metal nitrides (TMNs) are known to form more than one nitride[11]. Ni, which shares the same group with Pt, and Au which shares the same period with Pt in the periodic table, are known to form Ni_3N and Au_3N nitrides. Thus, it is of interest to consider more Pt atoms in the unit cell and less symmetric structures, and to know whether platinum can form Pt_3N with the reported structures of these and other 3:1 TMNs. In this work, the hypothetical Pt_3N is studied in the following seven structures: $D0_3$ (space group $Fm\bar{3}m$), A15 (space group $Pm\bar{3}n$), $D0_9$ (space group $Pm\bar{3}m$), $L1_2$ (space group $Pm\bar{3}m$), $D0_2$ (space group $Im\bar{3}$), ϵ-Fe_3N (space group $P6_322$) and RhF_3 (space group $R\bar{3}c$).

The following nine structures were assigned to PtN: B1 (space group $Fm\bar{3}m$), B2 (space group $Pm\bar{3}m$), B3 (space group $F\bar{4}3m$), $B8_1$ (space group $P6_3/mmc$), B_k (space group $P6_3/mmc$), B_h (space group $P\bar{6}m2$), B4 (space group $P6_3mc$), B17 (space group $P4_2/mmc$) and B24 (space group Fmmm). While C1 (space group $Fm\bar{3}m$), C2 (space group $Pa\bar{3}$), C18 (space group Pnnm) and $CoSb_2$ (space group $P2_1/c$) are the four structures which were proposed for PtN_2.

B. Electronic Relaxation Details

As implemented in the all-electron Vienna *ab initio* Simulation Package (VASP)[14–19], our electronic structure calculations were based on spin density functional theory (SDFT)[20,21]. To solve the self-consistent Kohn-Sham (KS) equations[22]

$$\left\{ -\frac{\hbar^2}{2m_e}\nabla^2 + \int d\mathbf{r}' \frac{n(\mathbf{r}')}{|\mathbf{r}-\mathbf{r}'|} + V_{ext}(\mathbf{r}) + V_{XC}^{\sigma,\mathbf{k}}[n(\mathbf{r})] \right\} \psi_i^{\sigma,\mathbf{k}}(\mathbf{r}) = \epsilon_i^{\sigma,\mathbf{k}} \psi_i^{\sigma,\mathbf{k}}(\mathbf{r}), \quad (1)$$

where i, $\mathbf{k}$ and σ are the band, $\mathbf{k}$-point and spin indices, respectively, the pseudo part of the KS orbitals $\psi_i^{\sigma,\mathbf{k}}(\mathbf{r})$ are expanded on plane-waves (PWs) basis. Only those PWs with kinetic energy $\frac{\hbar^2}{2m_e}|\mathbf{k}+\mathbf{G}| < E_{cut} = 600\ eV$ were included. This always corresponds to changes in the total electronic energy and in the so-called Fermi energy E_F that are less than 3 meV/atom and 1 meV, respectively.

For ionic relaxation, the Brillouin zones (BZs) were sampled using $13 \times 13 \times 13$ $\mathbf{\Gamma}$-centered Monkhorst-Pack meshes[23]; while for the static calculations, $17 \times 17 \times 17$ meshes were used. Any increase in the density of this mesh corresponds to change in the total energy and in Fermi energy E_F that are less than 2 meV/atom and 0.02 eV, respectively.

Partial occupancies were set using the tetrahedron method with Blöchl corrections[24–26] for the static total energy and the electronic density of states (DOS) calculations; while in the ionic relaxation, the smearing method of Methfessel-Paxton (MP)[27] was used. In the latter case, the smearing width was set such that the fictitious entropy is always less than 1 meV/atom.

The Perdew, Burke and Ernzerhof (PBE)[28–30] parametrization of the generalized gradient approximation (GGA)[31–33] was employed for the exchange-correlation potentials $V_{XC}^{\sigma,\mathbf{k}}[n(\mathbf{r})]$. VASP treats the core-valence interactions, $V_{ext}(\mathbf{r})$ using the projector augmented wave (PAW) method[19,34]. The PAW potential explicitly treats the $2s^2 2p^3$ electrons of N and the $5d^9 6s^1$ electrons of Pt as valence electrons.

In the standard mode of VASP, while fully relativistic calculations are performed for the core-electrons, only scalar kinematic effects are incorporated to treat the valance electronic structure[18]. It was found that this scheme is sufficient and the spin-orbit interactions have little effect on the macro-physical properties of platinum nitride[5]. Thus, we made no effort to consider spin-orbit coupling of the valence electrons.

The relaxation of the electronic degrees of freedom was performed using the blocked Davidson iteration scheme[35] as implemented in VASP. The electronic self-consistent (SC) convergence was considered to be achieved when the difference in the eigenvalues and in the total energy between two successive steps are both less than 1×10^{-4} eV.

C. Geometry Optimization and EOS

At a set of isotropically varying volumes of the unit cells, ions with internal free parameters were relaxed until all Hellmann-Feynman force components[36] on each ion were less than 1×10^{-2} $eV/$Å. Static total energy calculations (as described above) at each volume followed and the cohesive energy per atom was calculated from[37,38]

$$E_{coh}^{\mathrm{Pt}_m\mathrm{N}_n} = \frac{E_{\mathrm{solid}}^{\mathrm{Pt}_m\mathrm{N}_n} - Z\times\left(mE_{\mathrm{atom}}^{\mathrm{Pt}} + nE_{\mathrm{atom}}^{\mathrm{N}}\right)}{Z\times(m+n)}. \quad (2)$$

Here, Z is the number of $\mathrm{Pt}_m\mathrm{N}_n$ per unit cell, $E_{\mathrm{atom}}^{\mathrm{Pt}}$ and $E_{\mathrm{atom}}^{\mathrm{N}}$ are the energies of the spin-polarized non-spherical isolated Pt and N atoms, $E_{\mathrm{solid}}^{\mathrm{Pt}_m\mathrm{N}_n}$ are the bulk cohesive energies calculated by VASP with respect to spherical non spin-polarized reference atoms, and $m,n=1,2$ or 3 are the stoichiometric weights.

The calculated E_{coh} per atom as a function of volume V per atom were fitted to a Birch-Murnaghan 3rd-order equation of state (EOS)[39]

$$E(V) = E_0 + \frac{9V_0B_0}{16}\left(\left[\left(\frac{V_0}{V}\right)^{\frac{2}{3}}-1\right]^3 B_0' + \left[\left(\frac{V_0}{V}\right)^{\frac{2}{3}}-1\right]^2\left[6-4\left(\frac{V_0}{V}\right)^{\frac{2}{3}}\right]\right). \quad (3)$$

The four equilibrium fitting parameters: the equilibrium volume V_0, the equilibrium cohesive energy E_0, the equilibrium bulk modulus

$$B_0 = -V\frac{\partial P}{\partial V}\Big|_{V=V_0} = -V\frac{\partial^2 E}{\partial V^2}\Big|_{V=V_0} \quad (4)$$

and its pressure derivative

$$B_0' = \frac{\partial B}{\partial P}\Big|_{P=0} = \frac{1}{B_0}\left(V\frac{\partial}{\partial V}(V\frac{\partial^2 E}{\partial V^2})\right)\Big|_{V=V_0} \quad (5)$$

were determined by a least-squares method.

D. Formation Energy

In addition to E_{coh}, another important measure of relative stability is the so-called formation energy E_f. Assuming that the solid $\mathrm{Pt}_m\mathrm{N}_n$ results from the interaction between the solid Pt(fcc) metal and the gaseous N_2 through the chemical reaction

$$m\mathrm{Pt}^{\mathrm{solid}} + \frac{n}{2}\mathrm{N}_2^{\mathrm{gas}} \rightleftharpoons \mathrm{Pt}_m\mathrm{N}_n^{\mathrm{solid}}, \quad (6)$$

E_f can be obtained from

$$E_f(\mathrm{Pt}_m\mathrm{N}_n^{\mathrm{solid}}) = E_{\mathrm{coh}}(\mathrm{Pt}_m\mathrm{N}_n^{\mathrm{solid}}) - \frac{mE_{\mathrm{coh}}(\mathrm{Pt}^{\mathrm{solid}}) + \frac{n}{2}E_{\mathrm{coh}}(\mathrm{N}_2^{\mathrm{gas}})}{m+n}. \quad (7)$$

where $m,n=1,2,3$ are the stoichiometric weights and $E_{\mathrm{coh}}(\mathrm{Pt}_m\mathrm{N}_n^{\mathrm{solid}})$ is the cohesive energy per atom as obtained from Eq. 2. The ground-state cohesive energy and other equilibrium properties of the elemental platinum $E_{\mathrm{coh}}(\mathrm{Pt}^{\mathrm{solid}})$ in its fcc A1 structure (space group $\mathrm{Fm\bar{3}m}$ No. 225)[40–42] are given in Table I. We found the equilibrium cohesive energy of the molecular nitrogen ($E_{\mathrm{coh}}(\mathrm{N}_2^{\mathrm{gas}})$) and its N–N bond length to be -5.196 $eV/$atom and 1.113 Å. For details on how these properties were calculated, readers are referred to Ref. 43.

E. GWA Calculations and Optical Properties

Accurate quantitative description of optical properties of materials requires treatments beyond the level of DFT[44]. One choice is to follow the method which is provided by the many-body perturbation theory (MBPT). In this approach one needs to solve a system of quasiparticle (QP) equations[45–47]

$$\left\{-\frac{\hbar^2}{2m}\nabla^2 + \int d\mathbf{r}'\frac{n(\mathbf{r}')}{|\mathbf{r}-\mathbf{r}'|} + V_{ext}(\mathbf{r})\right\}\psi_{i,\mathbf{k}}^{QP}(\mathbf{r}) + \int d\mathbf{r}'\Sigma(\mathbf{r},\mathbf{r}';\epsilon_{i,\mathbf{k}}^{QP})\psi_{i,\mathbf{k}}^{QP}(\mathbf{r}') = \epsilon_{i,\mathbf{k}}^{QP}\psi_{i,\mathbf{k}}^{QP}(\mathbf{r}). \quad (8)$$

In practice, one takes the wave functions $\psi_{i,\mathbf{k}}^{QP}(\mathbf{r})$ from the DFT calculations. However, this technique is computationally expensive, and we had to use less dense meshes of $\mathbf{k}$-points: $(10\times10\times10)$ in the case of B17 and $(12\times12\times12)$ in the case of B3. The quantity $\Sigma(\mathbf{r},\mathbf{r}';\epsilon_{i,\mathbf{k}}^{QP})$ in Eqs. 8 above is known as self-energy. It contains all the static and dynamic exchange and correlation effects, including those neglected at the DFT-GGA level. When Σ is written in terms of the Green's function G and the frequency-dependent screened Coulomb interaction W as

$$\Sigma_{GW} = j\int d\epsilon' G(\mathbf{r},\mathbf{r}';\epsilon,\epsilon')W(\mathbf{r},\mathbf{r}';\epsilon), \quad (9)$$

the approximation is referred to as GW approximation. The dynamically screened interaction W is related to the bare interaction v via

$$W(\mathbf{r},\mathbf{r}';\epsilon) = j\int d\mathbf{r}_1\varepsilon^{-1}(\mathbf{r},\mathbf{r}_1;\epsilon)v(\mathbf{r}_1,\mathbf{r}'), \quad (10)$$

where the dielectric matrix ε is calculated within the random phase approximation (RPA). The QP eigenvalues

$$\epsilon_{i,\mathbf{k}}^{QP} = \mathrm{Re}\left(\left\langle\psi_{i,\mathbf{k}}^{QP}\middle|H_{\mathrm{KS}} - V_{XC} + \Sigma_{GW_0}\middle|\psi_{i,\mathbf{k}}^{QP}\right\rangle\right) \quad (11)$$

are updated in the calculations of G, while W is kept at the DFT-RPA level. This is called the GW_0 self-consistent routine on G. After the execution of the fourth iteration, ε is recalculated within the RPA using the updated QP eigenvalues[46–48]. It is straightforward then to calculate all the frequency-dependent optical spectra (e. g. refractive index $n(\omega)$, extinction coefficient $\kappa(\omega)$, absorption coefficient $\alpha(\omega)$, reflectivity $R(\omega)$ and transmitivity $T(\omega) = 1 - R(\omega)$) from the real $\varepsilon_{\rm re}(\omega)$ and the imaginary $\varepsilon_{\rm im}(\omega)$ parts of $\varepsilon_{\rm RPA}(\omega)$[49–51]:

$$n(\omega) = \frac{1}{\sqrt{2}}\left(\left[\varepsilon_{\rm re}^2(\omega) + \varepsilon_{\rm im}^2(\omega)\right]^{\frac{1}{2}} + \varepsilon_{\rm re}(\omega)\right)^{\frac{1}{2}} \quad (12)$$

$$\kappa(\omega) = \frac{1}{\sqrt{2}}\left(\left[\varepsilon_{\rm re}^2(\omega) + \varepsilon_{\rm im}^2(\omega)\right]^{\frac{1}{2}} - \varepsilon_{\rm re}(\omega)\right)^{\frac{1}{2}} \quad (13)$$

$$\alpha(\omega) = \sqrt{2}\omega\left(\left[\varepsilon_{\rm re}^2(\omega) + \varepsilon_{\rm im}^2(\omega)\right]^{\frac{1}{2}} - \varepsilon_{\rm re}(\omega)\right)^{\frac{1}{2}} \quad (14)$$

$$R(\omega) = \left|\frac{\left[\varepsilon_{\rm re}(\omega) + j\varepsilon_{\rm im}(\omega)\right]^{\frac{1}{2}} - 1}{\left[\varepsilon_{\rm re}(\omega) + j\varepsilon_{\rm im}(\omega)\right]^{\frac{1}{2}} + 1}\right|^2 \quad (15)$$

It may be worth to emphasize here that for more accurate optical properties (e.g. more accurate amplitudes and positions of the characteristic peaks), electron-hole excitations should be calculated by solving the so-called Bethe-Salpeter equation, the equation of motion of the two-body Green function G_2. The latter can be evaluated on the basis of our obtained GW one-particle Green function G and QP energies[52].

III. RESULTS AND DISCUSSION

Cohesive energy $E_{\rm coh}$ versus atomic volume V_0 equation of state (EOS) for the different phases of Pt_3N, PtN_2 and PtN are displayed graphically in Fig. 1, Fig. 2 and Fig. 3, respectively. The corresponding obtained equilibrium structural parameters and energetic and elastic properties are presented in Table I. In this table, as well as in Fig. 4, structures are first grouped according to the nitrogen content, starting with the stoichiometry with the lowest nitrogen content Pt_3N, followed by the 1:1 series and ending with the nitrogen-richest PtN_2 group. Within each series, structures are ordered according to their structural symmetry, starting from the highest symmetry (i.e. the highest space group number) to the least symmetry. Whenever possible, our results are compared with experiment and with previous calculations. In the latter case, the calculations methods and the XC functionals are indicated in the Table footnotes.

To study the effect of nitridation on the elemental Pt(A1) and to easly compare the properties of these phases relative to each other, the calculated equilibrium properties are displayed relative to the corresponding ones of Pt(A1) in Fig. 4.

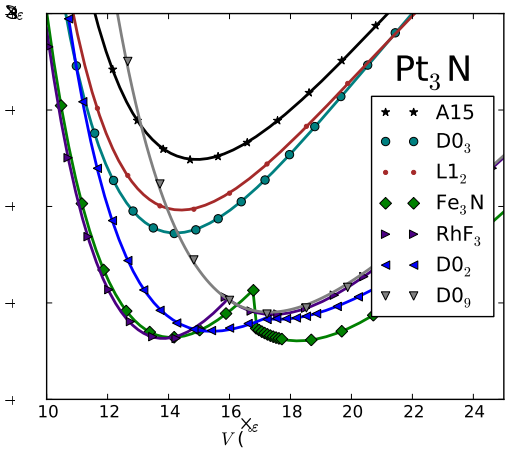

FIG. 1. (Color online.) Cohesive energy $E_{\rm coh}(eV/\text{atom})$ versus atomic volume V (Å^3/atom) for Pt_3N in seven different structural phases.

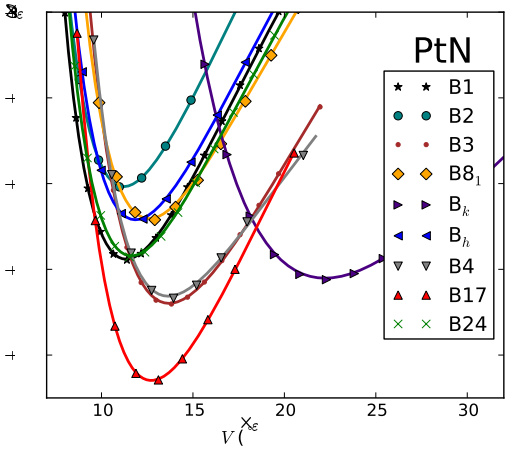

FIG. 2. (Color online.) Cohesive energy $E_{\rm coh}(eV/\text{atom})$ versus atomic volume V (Å^3/atom) for PtN in nine different structural phases.

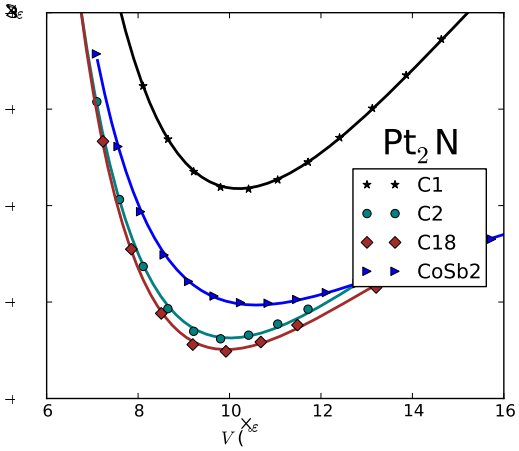

FIG. 3. (Color online.) Cohesive energy $E_{coh}(eV/\text{atom})$ versus atomic volume $V(\text{Å}^3/\text{atom})$ for PtN_2 in four different structural phases.

TABLE I. The calculated (*Pres.*) zero-pressure properties of the platinum nitrides and the results of previous calculations (*Comp.*). The available experimental data are given in the last row.

		$a(\AA)$	$b(\AA)$	$c(\AA)$	$\alpha(^\circ)$ or $\beta(^\circ)$	$V_0(\AA^3/\text{atom})$	$E_{\text{coh}}(eV/\text{atom})$	B_0(GPa)	B_0'	$E_f(eV/\text{atom})$
					Pt					
A1	*Pres.*	3.978	–	–	–	15.74	−5.451	242.999	5.486	
	Expt.	(3.9233 ± 0.0007)[a]	–	–	–	15.097[b]	−5.84[c]	278.3[c], 280[d]	5.18[e]	
		3.924[ee]	–	–	–			249[ee]	5.23[ee]	
	Comp.	3.90[g], 3.890[s], 3.981[gg],	–	–	–		−7.04[h], −3.74[i],	305[g], 320[s], 238[t]	5.16[k], 5.30[l], 5.25[m]	
		3.967[t], 3.966[cc]	–	–	–		−5.53[j]	249[cc], 242[dd], 244.18[gg]	5.23[cc], 5.83[dd], 5.7[gg]	
					Pt_3N					
$D0_3$	*Pres.*	6.106	–	–	–	14.23	−4.140	218.097	5.282	1.247
A15	*Pres.*	4.924	–	–	–	14.92	−3.759	194.136	5.266	1.628
$D0_9$	*Pres.*	4.114	–	–	–	17.41	−4.558	167.839	5.241	0.829
$L1_2$	*Pres.*	3.863	–	–	–	14.41	−4.021	205.279	5.472	1.366
$D0_2$	*Pres.*	7.875	–	–	–	15.26	−4.644	147.174	12.098	0.743
ϵ-Fe_3N	*Pres.*	5.680	–	5.293	–	18.49	−4.713	217.035	6.779	0.674
RhF_3	*Pres.*	5.463	–	–	$\alpha = 58.640$	13.97	−4.688	224.419	5.412	0.699
					PtN					
B1	*Pres.*	4.495	–	–	–	11.35	−3.945	230.869	5.059	1.378
		4.45[x], 4.50[y], 4.41[z]	–	–	–			232[x], 230[y], 288[z]		
	Comp.	4.471[cc]	–	–	–	10.66[ff]		251[cc], 242[dd], 294[ff]	4.00[cc], 4.78[dd]	1.365[cc]
		4.491[gg]	–	–	–			229.76[gg]	4.9[gg]	$[0.375 + E_f(B17)]$[hh]
B2	*Pres.*	2.819	–	–	–	11.20	−3.522	238.187	5.070	1.801
	Comp.	2.818[gg]	–	–	–			234.88[gg]	5.1[gg]	
B3	*Pres.*	4.782	–	–	–	13.67	−4.203	193.466	5.031	1.120
		4.7217[n], 4.8250[o], 4.779[gg],	–	–	–			243.3[n], 196.3[o], 190.61[gg],	5.1[gg],	
	Comp.	4.6833[p], 4.7889[q], 4.8114[r],	–	–	–			271.9[p], 192.7[q], 184[r],		0.95[aa]
		4.692[s], 4.780[t], 4.760[cc],	–	–	–			244[s], 194[t], 213[cc],	4.00[cc]	1.1[cc]
		4.80[x,y], 4.70[z], 4.699[hh]	–	–	–			192[x], 190[y], 232[z], 217[dd]	3.62[dd]	$[0.21 + E_f(B17)]$[hh]
$B8_1$	*Pres.*	3.482	–	4.843	–	12.71	−3.713	210.165	4.945	1.610
B_k	*Pres.*	3.378	–	8.986	–	22.20	−4.061	108.968	4.553	1.262
B_h	*Pres.*	3.039	–	2.966	–	11.86	−3.716	222.279	5.014	1.607
B4	*Pres.*	3.382	–	5.539	–	13.72	−4.171	190.130	5.033	1.152
	Comp.	3.386[gg]	–	5.529[gg]	–			191.06[gg]	4.7[gg]	
B17	*Pres.*	3.069	–	5.403	–	12.72	−4.652	235.041	5.018	0.671
	Comp.	3.323[hh]	–	4.579[hh]	–					
B24	*Pres.*	4.216	4.472	4.948	–	11.66	−3.928	226.608	5.153	1.395
	Comp.[*]	3.972[hh]	3.977[hh]	6.022[hh]	–			270[hh]		$[0.085 + E_f(B17)]$[hh]
					PtN_2					
C1	*Pres.*	4.963	–	–	–	10.19	−3.918	263.295	4.717	1.363
	Comp.	4.9428[n], 5.0403[o],	–	–	–			322.1[n], 267.2[o], 269[cc],	4.00[cc]	1.167[aa]
		4.866[s], 4.958[t], 4.939[dd]	–	–	–			316[s], 264[t], 260[dd]	4.73[dd]	1.317[dd]
C2	*Pres.*	4.912	–	–	–	9.882	−4.689	226.779	6.893	0.592
	Comp.	4.87[aa]	–	–	–	9.12[ff]				0.267[aa], 0.24[bb]
		4.848[cc], 4.874[ii]	–	–	–	9.65[ii]		305[cc], 285[dd], 300[ii]	4.00[cc], 5.50[dd]	0.64[cc], 0.212[ii]
C18	*Pres.*	3.036	3.984	4.862	–	9.800	−4.755	244.320	7.938	0.526
	Comp.	3.778[ii]	4.880[ii]	3.208[ii]	–	9.827[ii]		286[ii]		0.249[ii]
$CoSb_2$	*Pres.*	5.460	5.163	9.374	$\beta = 151.225$	10.60	−4.508	118.594	6.619	0.773
	Comp.	4.950[ii]	4.880[ii]	4.950[ii]	99.50[ii]	9.827[ii]		289[ii]		0.248[ii]
					Experiment					
		(4.8032 ± 5)[u,v], 4.8041(2)[w]	–	–	–			(372 ± 5)[u], (354 ± 5)[v]	4.0[u], 5.26[v]	

[a] Ref. 53: This is an average of 23 experimental values, at room temperature.
[b] Ref. 53: at room temperature.
[c] Ref. 54: Cohesive energies are given at 0 K and 1 atm = 0.00010 GPa; while bulk moduli are given at room temperature.
[d] Ref. (25) in 55: at room temperature.
[e] See Refs. (8)–(11) in 55.
[g] Ref. 56: using the full-potential linearized augmented plane waves (LAPW) method within LDA.
[h] Ref. 57: using the projector augmented wave (PAW) method within LDA.
[i] Ref. 57: using the projector augmented wave (PAW) method within GGA(PW91).
[j] Ref. 57: using the projector augmented wave (PAW) method within GGA(PBE).
[k] Ref. 55: using the so-called method of transition metal pseudopotential theory; a modified form of a method proposed by Wills and Harrison to represent the effective interatomic interaction.
[l] Ref. 55: using a semi-empirical estimate based on the calculation of the slope of the shock velocity *vs.* particle velocity curves obtained from the dynamic high-pressure experiments. The given values are estimated at ~ 298 K.
[m] Ref. 55: using a semi-empirical method in which the experimental static $P - V$ data are fitted to an EOS form. The given values are estimated at ~ 298 K.
[n] Ref. 5: using the ultrasoft pseudopotential (USPP) method within LDA. B_0's are calculated from elastic constants.
[o] Ref. 5: using the ultrasoft pseudopotential (USPP) method within GGA. B_0's are calculated from elastic constants.
[p] Ref. 5: using the projector augmented wave (PAW) method within LDA. B_0' is set to be 4.
[q] Ref. 5: using the projector augmented wave (PAW) method within GGA. B_0' is set to be 4.
[r] Ref. 5: using fully relativistic full-potential linearized augmented plane waves (LAPW) method within GGA.
[s] Ref. 8: using the full-potential linearized augmented plane waves (LAPW) method within LDA.
[t] Ref. 8: using the full-potential linearized augmented plane waves (LAPW) method within GGA(PBE).
[u] Ref. 1: The experimental evolution of the volume with pressure was fitted with a Birch-Murnaghan EOS, but B_0' was set to be 4.
[v] Ref. 1: The experimental evolution of the volume with pressure was fitted with a Birch-Murnaghan EOS, but $B_{0,\text{Pt}}' = 5.26$ was fixed.
[w] Ref. 1: From XRD measurements at 0.1 MPa.
[x] Ref. 9: using the full-potential linearized augmented plane waves (FPLAPW) method within GGA(PBE).
[y] Ref. 9: using pseudopotentials method within GGA(PBE).
[z] Ref. 9: using pseudopotentials method within LDA.
[aa] Ref. 4: using the PAW method within GGA(PW91), but the experimental value of $E_{\text{coh}}(N_2^{\text{gas}})$ in Eq. 7 was used.
[bb] Ref. 4: using the full-potential linear-augmented plane-wave method.
[cc] Ref. 6: using pseudopotentials method within GGA(PBE).
[dd] Ref. 6: using pseudopotentials method within GGA(PBE).
[ee] Ref. 58.
[ff] Ref. 7: using the pseudopotential method within LDA.

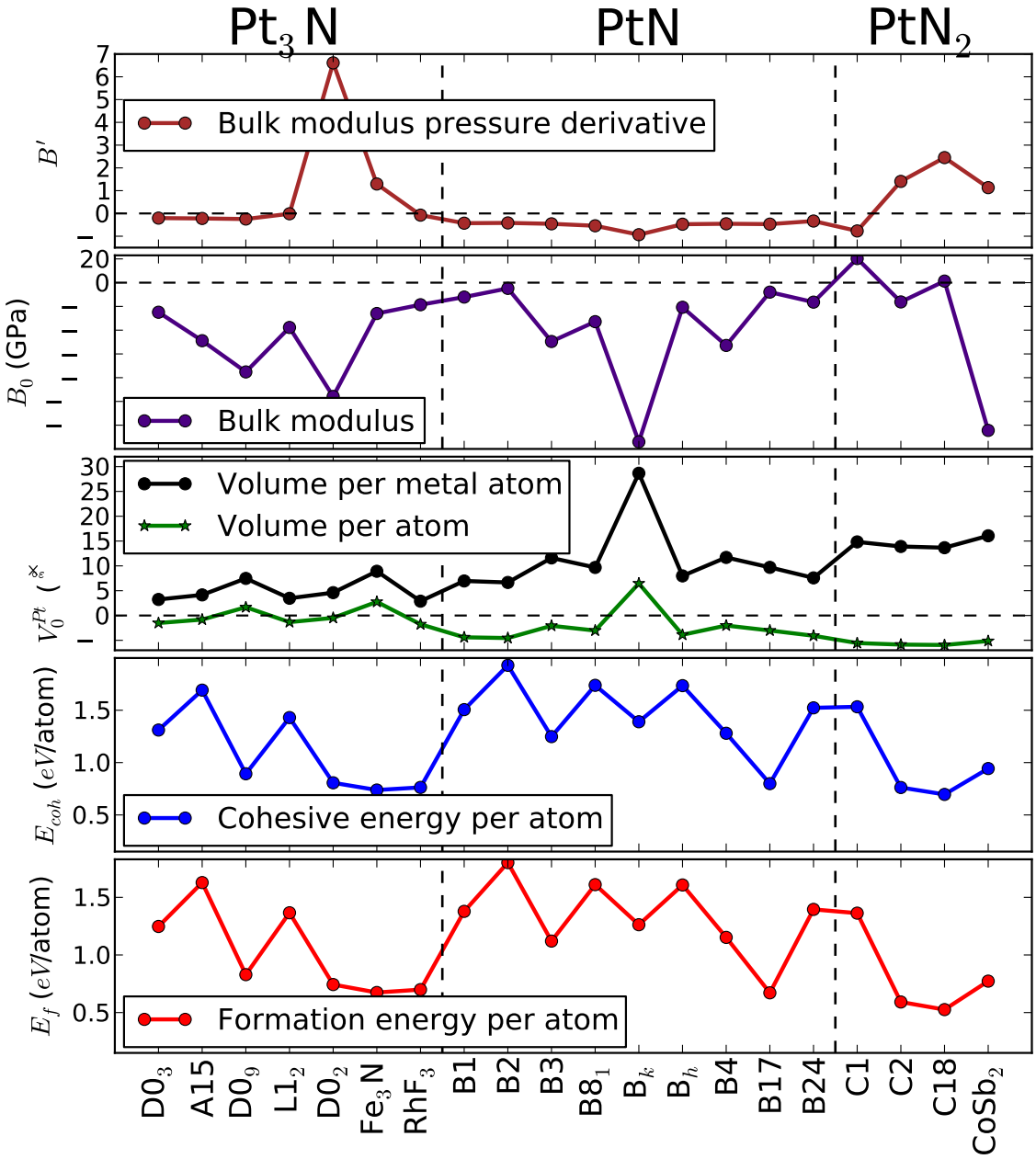

FIG. 4. (Color online.) Calculated equilibrium properties of the twenty studied phases of platinum nitrides. All quantities are given relative to the corresponding ones of the *fcc* crystalline elemental platinum given in the first row of Table I.

A. EOS and Relative Stabilities

Fig. 1 reveals that Pt_3N in its least symmetric phase, the trigonal (rhombohedric) structure of RhF_3, is the most favorable phase in this series. However, after ~ 15.9 Å^3/atom the EOS of $Pt_3N(RhF_3)$ is almost identical with the EOS of Pt_3N in the simple cubic structure of the anti-ReO_3 ($D0_9$). They share a minimum at $\sim$ (17.4 Å^3/atom, -4.56 eV). Very close to this point, at $\sim$ (17.23 Å^3/atom, -4.59 eV), the EOS of $Pt_3N(D0_2)$ has a kink due to a change in the positions of some Pt ions.

The EOS of $Pt_3N(Fe_3N)$ has two minima located at (14.11 Å^3/atom, -4.697 eV) and (18.26 Å^3/atom, -4.679 eV). Thus, the two minima are very close in energy but, due to the difference in V_0, they correspond to bulk moduli of 222.7 GP and 169.0 GP, respectively. The Pt ions are in the $6g$ Wyckoff positions: $(x,0,0),(0,x,0),(-x,-x,0),(-x,0,\frac{1}{2}),(0,-x,\frac{1}{2})$ and $(x,x,\frac{1}{2})$. Upon ion relaxation of $Pt_3N(Fe_3N)$, atomic positions change from $x\sim\frac{1}{3}$ to $x=\frac{1}{2}$ causing the sudden change in the potential surface (at $\sim$ 16.83 Å^3/atom) as the bulk $Pt_3N(Fe_3N)$ being decompressed (Fig. 1). It may be worth mentioning here that $Ag_3N(Fe_3N)$[61] and $Cu_3N(Fe_3N)$[43] were found to behave in a similar manner.

Hence, one of the two minima in the EOS of $Pt_3N(RhF_3)$ is shared with the minimum of the EOS of $Pt_3N(D0_9)$ and the other is shared with one of the two minima of $Pt_3N(Fe_3N)$.

The crossings of the less stable $D0_3$, $L1_2$ and A15 EOS curves with the more stable $D0_9$ EOS at the left side of their equilibria indicates that $D0_9$ would not survive under pressure and that possible pressure-induces phase transitions from the latter phase to the former ones may occur.

Fig. 4 shows that the Pt_3N most stable phases may energetically compete with the PtN and PtN_2 most stable ones. However, from the foregoing discussion, it seems that Pt_3N would not have a simple potential surface.

Using the full potential augmented plane wave plus local orbitals (APW+lo) method within GGA(PBE), the energy-volume EOS's for B1, B2, B3 and B4 have been studied by the authors of Ref. 59. Some of their obtained equilibrium properties are included and referred to in Table I. Within the considered parameter sub-space, our obtained EOS's (Fig. 2), relative stabilities, and equilibrium structural parameters and mechanical properties (Table I) are in excellent agreement with their findings. However, relaxing the c/a parameter, they obtained an additional EOS which lies below all the other considered ones, but its equilibrium B_0 is significantly smaller.

From Fig. 2, it is evident that PtN(B17) is the energetically most stable phase in the PtN series. The difference in the equilibrium $E_{\rm coh}$ between PtN(B17) and the next (less) stable phase, PtN(B3), is about 0.5 eV (Table I). This difference was found by other researchers[9] to be $0.9-1.05$ eV. The crossings of the EOS curve of B17 with some of those of less stability at the left side of their equilibria reveals possible pressure-induces phase transitions. To closely investigate these transitions, we plot the corresponding relations between enthalpy $H=E(V)+PV$ and the imposed external pressure P. Possible transitions and the pressures at which they occur are carefully depicted. A point where two $H(P)$ curves (of two modifications with the same chemical stoichiometry[7]) meet represents a phase transition from the phase with the higher H to the one with the lower H[37]. From the $H(P)$ diagrams (not shown here) we found that PtN(B17) would transform to PtN(B1, B2, B_h or B24) at $\sim$ 93 GPa, $\sim$ 143 GPa, $\sim$ 193 GPa or $\sim$ 123 GPa, respectively.

It may be worth to mention here a few points about this B17 structure: (i) It was theoretically predicted to be the ground-state structure of CuN[43], AgN[61], AuN[62] and PdN[63]. (ii) The same foregoing phase PtN-PtN structural pressure-induced transitions have been predicted for PdN, but at relatively smaller pressures in the range (25.8 $\sim$ 62.1 GPa)[63]. (iii) B17 is the structure of PtS[64] and PtO[9]. (iv) It was found by other authors to be a possible ground state for PtN[9]. (v) The B17 structure has an fcc Pt sub-lattice (as the synthesized platinum nitride), but it is tetragonal and the sub-lattice are highly distorted ($c/a\approx\sqrt{3}$ versus $c/a=\sqrt{2}$ for ideal fcc), and probably because of this distortion it was rejected by the platinum nitride synthesizers[1]. (vi) Fig. 5 that B17 is energetically favorable over B1 and B3 at all pressures.

Nevertheless, PtN(B17) was found to be elastically unstable[10].

Assuming 1:1 stoichiometry, the first platinum nitride synthesizers assigned the B3 structure for their product[1]. However, it was shown in the same work that PtN(B3) should break down or transform at pressures above 12 GPa. In agreement with this experimental prediction, Fig. 5 shows that PtN(B3) would not survive at pressures above 19 GPa where the B3→B1 phase transition occurs. Other theoretical works also predicted that B1 becomes more favorable than B3 structure above 13.3 GPa[9], $\sim$ 15 GPa[7], 16.5 GPa[9], and 17.6 GPa[9].

Therefore, we support Ref. 9 on the judgment that, unless the PtN(B3) was formed upon depressurization, its production at $45-50$ GPa[1] is questioned. Further, first-principles calculations showed that PtN(B3) is elastically unstable[5,6,8], and that it may distort spontaneously to a tetragonal lattice to lower the energy[8].

In the PtN_2 series, we can see from Table I and from Fig. 4 that PtN_2 in the simple orthorhombic structure of FeS_2 marcasite (C18) is the most stable phase, while the face-centered cubic structure of CaF_2 fluorite (C1) is significantly the least favorable structure. Yet, Fig. 5 reveals that the latter PtN_2(C1) is more favorable than the proposed PtN(B1, B3 and B17) at pressures above

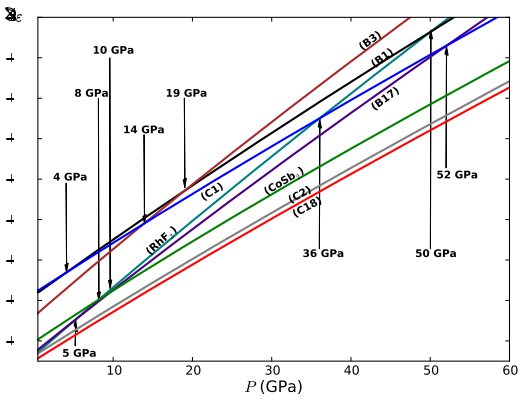

FIG. 5. (Color online.) Enthalpy H *vs.* pressure P equation of state (EOS) for the most favorable Pt_3N phase (RhF_3), the three proposed PtN modifications (B1, B3 and B17), and the four considered PtN_2 structures in the present work (C1, C2, C18 and $CoSb_2$). The arrows indicate the pressures at which curves cross each other.

4 GPa, 14 GPa and 52 GPa, respectively. Others[9] found PtN_2(C1) to be more favorable than PtN(B3) at pressures above 30 GPa.

In contrast to our enthalpy-pressure EOS's in Fig. 5, Chen, Tse and Jiang[60] obtained an $H(P)$ curve for C18 which lies always above the curve for C2 and coincides with the one of $CoSb_2$. They concluded that C2 is the most stable structure among these three modifications. While we sticked to the original C18 relative dimensions, it seems that Chen, Tse and Jiang tried to optimize the lattice parameters ratios (see Table I). However, the $c : a : b$ ratio they obtained is very close to our $a : b : c$ ratio, and the difference in V_0 is less than 0.03 $Å^3$/atom)[65]. Another difference is the atomic electronic configuration of Pt $5d^8 6s^2$ they used. Nevertheless, they agreed with us that in the $0-60$ GPa pressure range, no transition between these three phases occurs.

Comparing the relative stability of the three most stable compositions, we find from Table I and from Fig. 4 that PtN_2(C18) is the most favorable, followed by Pt_3N(RhF_3), and the least stable phase is PtN(B17). However, the differences in their equilibrium $E_{\rm coh}$ lies within a narrow range of 0.036 eV. Relative to their parent metal, all phases have higher $E_{\rm coh}$, i.e. they are less bound than Pt(A1). Hence, we found, as other theoretical works[8], that platinum nitride can be stabilized in stoichiometries and structures other than that proposed by the first synthesizers[1].

In Ref. 9, the energy-volume EOS for B1, B3, B17, C1, and C2 have been studied using DFT-GGA. Within this parameter sub-space, our obtained EOS's (Figs. 2, 3 and 4) are in excellent agreement with the findings of 9. From the relative enthalpy-pressure diagrams[66], Ref. 9 arrived at an astonishing result: the experimentally proposed PtN(B3) is an entirely unstable structure at any pressure.

To closely study the non-zero pressure stoichiometric and structural preferences, we displayed in Fig. 5 the enthalpy H *vs.* pressure P equation of states (EOS) for the most favorable Pt_3N phase (RhF_3), the three previously proposed PtN modifications (B1, B3 and B17), and the four considered PtN_2 structures in the present work (C1, C2, C18 and $CoSb_2$). The arrows indicate the pressures at which curves cross each other. From these curves, it is clear that PtN_2(C18), followed by PtN_2(C2), are the most energetically favorable phases at all pressure. At pressures above 10 GPa, PtN_2($CoSb_2$) has lower enthalpy than the rest of the modifications, including PtN(B17) and PtN_2(C1). At pressures higher than 8 GPa, PtN(B17) becomes more favorable than Pt_3N(RhF_3), but the former never competes behind 52 GPa when PtN_2(C1) becomes more favorable. However, Pt_3N(RhF_3) is more stable than PtN(B3) at all pressures. In summary, Fig. 5 reveals that even if a PtN phase has been observed (at pressures around 50 GPa), this phase must be unstable toward phase decomposition into solid constituents Pt and PtN_2 (see also Ref. 7) or into Pt and Pt_3N. However, the series of the possible phase transitions must be carefully investigated.

B. Volume per Atom and Lattice Parameters

The obtained equilibrium volume per atom V_0, i.e. the inverse of the number density, for all the considered modifications are numerally presented in Table I and graphically depicted relative to the Pt(A1) in Fig. 4. On average, Pt_3N phases tend not to change the number density of the host parent Pt(A1); PtN phases tend to slightly increase it; while the PtN_2 increase it significantly.

It is also evident from Fig. 4 that in crossing the boarders between the Pt_3N and PtN and between the PtN and PtN_2 islands, i.e. in increasing the N content, V_0 tends to decrease while the volume per Pt atom $V_0^{\rm Pt}$, a measure of the average Pt–Pt bond length, tends to increase. The latter finding has been found to be true for the nitrides of Cu[43] and Ag[61] as well.

C. Bulk Modulus and its Pressure Derivative

With only a few exceptions, Fig. 4 and Table I reveal that nitridation of Pt apparently tends to reduce its bulk modulus. Relative to each other, the twenty B_0's show no clear trend. The most energetically favorable PtN phase, B17, has 42 GPa higher bulk modulus than the proposed PtN(B3).

As we mentioned somewhere else[67], B_0 is far more sensitive to any change in volume than the change in $E_{\rm coh}$. The case of PtN(B2) is a clear example, in which the slight decrease in V_0 overcomes the significant increase in

$E_{\rm coh}$ leading only to a very small decrease in B_0 (Fig. 4 and Table I).

Given that all the considered phases have higher $E_{\rm coh}$ than Pt(A1), the foregoing argument fails to explain the decrease in B_0 in the case of the structures which have lower V_0 than their parent Pt(A1) and have lower $E_{\rm coh}$ than the extreme case PtN(B2). However, if one replaces V_0 in the argument above with $V_0^{\rm Pt}$, the contradiction can be lifted. Therefore, we believe that the mechanical properties in these nitrides may be dominated by the effect of the Pt-Pt bond length more than the simple number density.

Although the GGA calculated B_0 values in the present and previous works (Table I) are far smaller than the reported experimental value, our obtained bulk modulus for PtN_2(C1) is 20 GPa higher than that of Pt(A1). This is exactly the measured value for Pt after the PtN formation took place. The observation was considered by Gregoryanz et al. as an indication that some N is dissolved in Pt[1]. Recalling that the B_0 of the produced platinum nitride is ~ 100 GPa than that of Pt(A1)[1], our GGA-obtained B_0 for PtN_2(C1) is ~ 80 GPa less than the experimental value[68].

It may be worth to notice from Table I that the lattice parameter a of PtN_2(C1) is 0.13 Å higher than that of PtN(B3); yet the B_0 of the former is ~ 70 GPa higher than the latter. This difference in B_0 can be attributed to the fact that in B3, N atoms occupy only half of the tetrahedral interstitial sites of the Pt sub-lattice, while in C1, the four remaining tetrahedral interstitial sites are filled with N atoms[8,9,69]. This filling significantly reduces the compressibility but slightly increases the volume of the unit cell. This fact can also be seen readily as a consequence of the difference in the average volume per atom in the two cases (Table I).

The pressure derivative of the bulk modulus, B_0', measures the sensitivity of B_0 to any external pressure. The top subfigure in Fig. 4 reveals that the bulk moduli of Pt_3N(Fe_3N) and PtN_2(C2, C18 and $CoSb_2$) increase upon application of external pressure. Pt_3N($D0_2$) is very sensitive and its B_0 will increase significantly under an infinitesimal excess of pressure. Pt_3N($L1_2$ and RhF_3) tend to be inert; while Pt_3N($D0_3$, A15 and $D0_9$), PtN_2(C1) and all PtN phases tend to decrease their bulk modulus upon application of external pressure. Although B_0' is a measurable quantity[55], we couldn't find any experimental value to test our obtained values against.

D. Formation Energies

From Fig. 4 and Table I, it is evident that formation energy E_f has the same trend as the cohesive energy $E_{\rm coh}$. If E_f is taken as a measure of synthesized, then the relatively most favorable Pt_3N phases have the same synthesized as the most favorable PtN and PtN_2.

A positive value of E_f means, in principle, that, at the temperature and pressure at which E_f is calculated, the phase is thermodynamically unstable (endothermic) and have a tendency to decompose into its constituent components. In our case, this observation is corroborated by the experimental fact that the synthesis of the platinum nitrides was achieved only at high temperature and temperature[6,60].

Using different methods, other researchers[4,6,60] also obtained positive (zero-pressure and zero-temperature) formation energies for some PtN and/or PtN_2 phases. Some of their values are included in Table I with indication to the methods of calculations.

The obtained relative difference in E_f for PtN_2(C1) and PtN_2(C2) is in good agreement with Ref. 4. However, the differences in our and their obtained E_f values can be attributed to three factors: First, the difference in the obtained lattice parameter (see Table I). Second, the value of our calculated equilibrium free parameter u is 0.417 while Ref. 4 obtained 0.415[70]. Third, and the most significant source of difference, the experimental value of $E_{\rm coh}(N_2^{\rm gas})$ in Eq. 7 was used by Ref. 4, while we calculated it as described in sub-section II D.

It may be worth mentioning here that a negative theoretical value of $E_f = -0.4$ eV/atom was obtained for PtN_2(C2) at $P = 50$ GPa, showing excellent agreement with experiment[4]. Moreover, Young et al.[6] claimed that PtN_2 dissociates upon mild heating below $P = 10$ GPa.

E. Electronic Properties

The DFT obtained band diagrams $\epsilon_i^\sigma(\mathbf{k})$ and spin-projected total and partial density of states (DOS) of the most stable modifications: Pt_3N(RhF_3), PtN(B3 and B17), and PtN_2(C18) are displayed in Figs. 6, 7, 8 and 9, respectively. Spin-projected total density of states (TDOS) are shown in sub-figure (b) in each case. Because in these four considered cases electrons occupy the spin-up and the spin-down bands equally, it was sufficient only to display spin-up DOS and spin-up band diagrams. Displaying the energy bands along densely sampled high-symmetry strings of $\mathbf{k}$-points allows us to extract information about the electronic structure of these phases. Moreover, to investigate the details of the orbital character of the bands, the Pt(s,p,d) and N(s,p) resolved DOS's are plotted at the same energy scale.

With The Fermi surface crossing the partly occupied bands. it is clear from Figs. 6, 7, and 8 that Pt_3N(RhF_3) PtN(B3) and PtN(B17) are metals.

The TDOS of Fig. 9(b) reveal that PtN_2(C18) is a semiconductor with (Fig. 9(a)) its valence band maximum (VBM) at $(Y, -0.091\ eV)$ and its conduction band minimum (CBM) at $(Y, 0.044\ eV)$, resulting in a narrow direct energy band gap $E_g = 0.135$ eV of width. Below this fundamental gap there are three bands: the deep one at ~ -20.5 eV consists mainly of the N$(2s)$ states. Its high DOS and sharp feature correspond to its little and slow energy variation in the $\mathbf{k}-$space. The second band

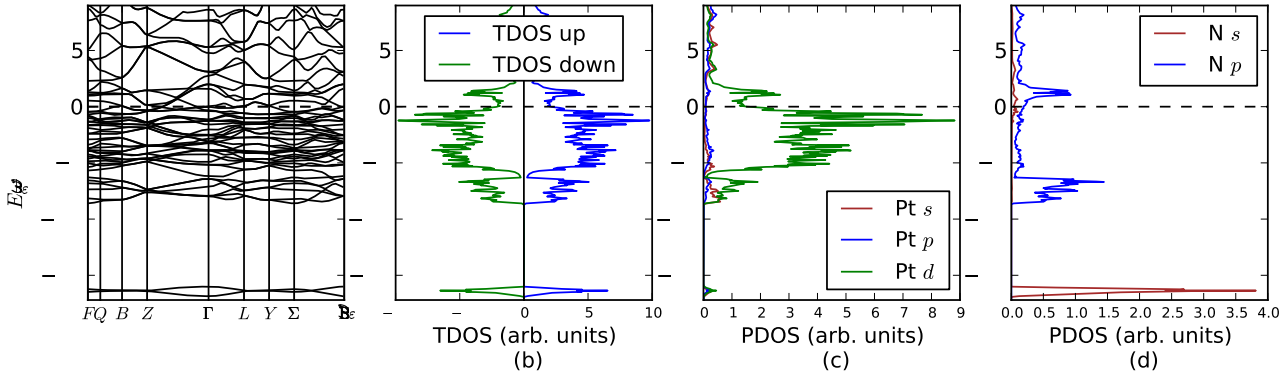

FIG. 6. (Color online.) DFT calculated electronic structure for Pt_3N in the RhF_3 structure: **(a)** band structure along the high-symmetry **k**-points which are labeled according to Ref. [71]. Their coordinates w.r.t. the reciprocal lattice basis vectors are: $F(0.5, 0.5, 0.0)$, $Q(0.375, 0.625, 0.0)$, $B(0.5, 0.75, 0.25)$, $Z(0.5, 0.5, 0.5)$, $\Gamma(0.0, 0.0, 0.0)$, $L(0.0, 0.5, 0.0)$, $Y(0.25, 0.5, -.25)$, $\Sigma(0.0, 0.5, -.5)$; **(b)** spin-projected total density of states (TDOS); **(c)** partial density of states (PDOS) of $Pt(s, p, d)$ orbitals in Pt_3N; and **(d)** PDOS of $N(s, p)$ orbitals in Pt_3N.

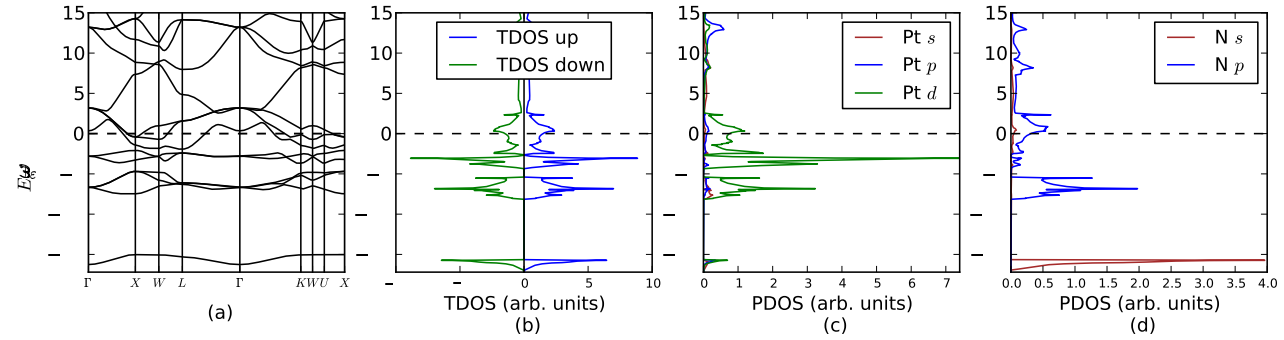

FIG. 7. (Color online.) DFT calculated electronic structure for PtN in the B3 structure: **(a)** band structure along the high-symmetry **k**-points which are labeled according to Ref. [71] [a]. Their coordinates w.r.t. the reciprocal lattice basis vectors are: $\Gamma(0.0, 0.0, 0.0)$, $X(0.0, 0.5, 0.0)$, $W(0.75, 0.25, 0.5)$, $L(0.5, 0.5, 0.5)$, $K(0.750, 0.375, 0.375)$, $U(0.625, 0.250, 0.625)$; **(b)** spin-projected total density of states (TDOS); **(c)** partial density of states (PDOS) of $Pt(s, p, d)$ orbitals in PtN; and **(d)** PDOS of $N(s, p)$ orbitals in PtN.

[a] ***The coordinates of the W point is not as the same as in Ref. [71], but they are equivalent. Also, the coordinates of U and K are not given in Ref. [71]. The coordinates of U, K and the equivalent W were created by means of XCrySDen!***

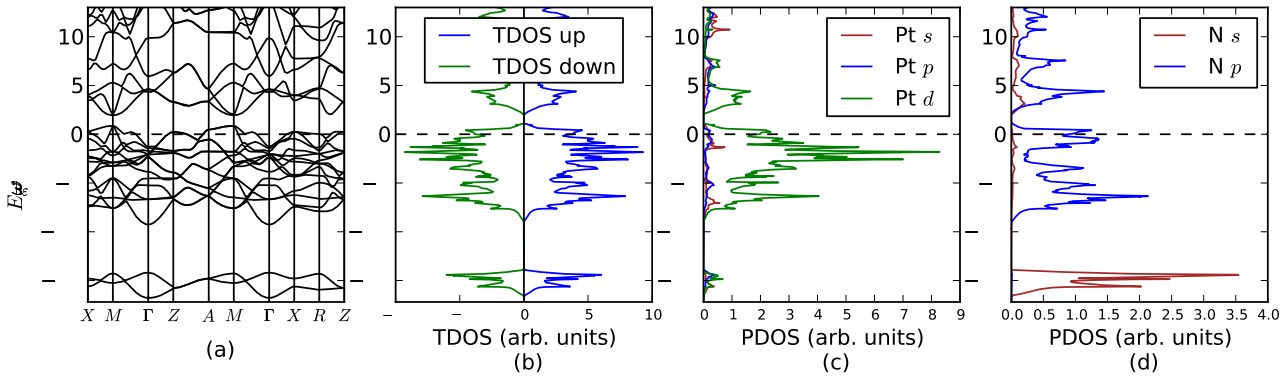

FIG. 8. (Color online.) DFT calculated electronic structure for PtN in the B17 structure: **(a)** band structure along the high-symmetry **k**-points which are labeled according to Ref. [71]. Their coordinates w.r.t. the reciprocal lattice basis vectors are: $X(0.0, 0.5, 0.0)$, $M(0.5, 0.5, 0.0)$, $\Gamma(0.0, 0.0, 0.0)$, $Z(0.0, 0.0, 0.5)$, $A(0.5, 0.5, 0.5)$, $R(0.0, 0.5, 0.5)$; **(b)** spin-projected total density of states (TDOS); **(c)** partial density of states (PDOS) of $Pt(s, p, d)$ orbitals in PtN; and **(d)** PDOS of $N(s, p)$ orbitals in PtN.

is relatively narrow ($\sim 2.2\ eV$ of width) with low density and steming mainly from a mixture of the N states with Pt(d) states. The superposition Pt(d) and N(p) states in the region from $-10.314\ eV$ to $-0.091\ eV$ below the fundamental gap constitutes the third band with highly structured, intense and narrow series of peaks. Our obtained TDOS and PDOS show excellent agreement with Ref. 60 where also PtN_2(C18) was predicted to be a semiconductor, but band diagrams and E_g value are not given.

It may be worth mentioning here that PtN(B1)[10] and PtN(B4)[59] were found to be metallic, PtN_2(C1) was found to be a poor metal[8], $PtN_2(CoSb_2)$[60] was found to be a semiconductor, and an indirect band gap between $1.2\ eV$[60] and $1.5\ eV$[6] has been obtained for PtN_2(C2).

F. Optical Properties

GW calculations were carried out for the PtN(B3) and PtN(B17) metallic phases at their equilibrium. Figs. 10 and 11 display the obtained real and imaginary parts of the frequency-dependent dielectric function $\varepsilon_{\rm RPA}(\omega)$ of these two phases and the corresponding derived optical spectra (Eqs. 12 – 15). In each sub-figure, the optical region [$\sim (3.183 - 1.655)\ eV \equiv (390 - 750)\ nm$] is shaded.

The non-vanishing absorption coefficient $\alpha\,(\omega)$ in the whole range for both phases confirms their metallic character. As it should be the case, refraction $n(\omega)$ and extinction $\kappa(\omega)$ coefficients behave as the real $\varepsilon_{\rm re}(\omega)$ and the imaginary $\varepsilon_{\rm im}(\omega)$ dielectric functions, respectively.

As one can see from sub-figure 10(d), close to the edge of the optical region at $\sim$ ($1.762\ eV = 703.768\ nm$) PtN(B3) is 50% reflector and 50% transmitter. From $\sim$ ($2.071\ eV = 598.579\ nm$) to the UV region, PtN(B3) is only $\sim 40\%$ reflecting but $\sim 60\%$ transmitting. However, more of the transmitted portion in this region will be absorbed as the photon energy increases. This fact can be readily noticed if one compares sub-figures 10(c) and 10(d).

PtN(B17), as can be seen from sub-figure 11(d), is a very good reflector in the whole region until $\sim$ ($3.000\ eV = 413.281\ nm$) where it equally reflects and transmits the violet light. However, less of the transmitted portion in the optical region will be absorbed as the photon wavelength decreases. This fact can be readily observed in sub-figures 11(c).

According to the best of our knowledge, there is no available experimental optical spectra for the platinum nitride. However, from their visual appearance, all the synthesized platinum nitride samples look very shiny and darker than their parent platinum in reflected light and totally opaque in transmitted light. These features suggest that PtN is either a poor metal or a semiconductor with a small band gap[1].

From Figs. 11 and 8, the above mentioned properties are strongly met by PtN(B17), but purely seen (Figs. 10 and 7) in PtN(B3), as discussed above. Unfortunately, we did not carry out optical calculations for PtN_2(C1 or C2).

G. PtN versus PtN_2

Using our own obtained results in the present work as well as the findings of other researchers, below we make a comparison between the PtN modifications (supported by the experimentalists) and the PtN_2 phases (supported by the theoreticians):

- Given that GGA calculated lattice parameters are usually overestimated[72–74], the obtained values of the a lattice parameter for PtN_2(C1 and C2) are the closest ones to the experimental value (to within 3 % and 2 %, respectively), while the PtN phases are in poor agreement with experiment, as can be seen in Table I.

- First-principles studies of transition metals nitrides show that the B_0's of the elemental metals are generally enhanced by nitridation[1,75]. Compared to experiment, Table I and Fig. 4 reveal that this trend is met by PtN_2(C1), while PtN(B3) has 50 GPa lower than Pt(A1).

- Like the first synthesized sample and the proposed PtN(B3) modification[1], PtN_2(C1[8] and C2[4]) have fcc sub-lattice of Pt.

- PtN_2(C1[8], C2[6,60], C18[60] and $CoSb_2$[60]) have all been found to be elastically stable, while PtN(B3[5,6,8,10] and B17[10]) were found to be elastically unstable.

- Formation and cohesive energies of PtN_2(C2, C18 and $CoSb_2$) are lower than that of PtN(B3) [Table I and Fig. 4].

- In excellent agreement with experiment, the calculated formation energy of PtN_2(C2) at $P = 50$ GPa was calculated to be negative[4], while calculations found PtN(B3) to be thermodynamically unstable at all pressures[9].

- The experimentally obtained Raman spectrum of the reproduced platinum nitride[4] matches closely that of pyrite (FeS2), i.e. in the C2 structure, but does not match the PtN(B3) spectrum that expected from group theory[4].

- The theoretically calculated[6,60] Raman spectrum for PtN_2(C2) shows good agreement with the first experimentally obtained one[1].

- In agreement with the experimental observation and the visual appearance of the first produced platinum nitrides[1], PtN_2(C1) was found to be a

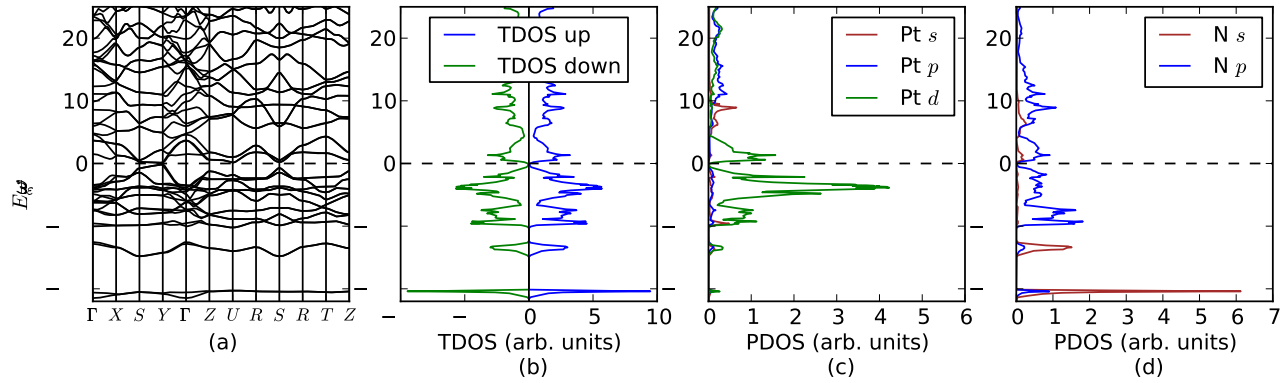

FIG. 9. (Color online.) DFT calculated electronic structure for PtN_2 in the C18 structure: **(a)** band structure along the high-symmetry **k**-points which are labeled according to Ref. [71]. Their coordinates w.r.t. the reciprocal lattice basis vectors are: $\Gamma(0.0, 0.0, 0.0)$, $X(0.0, 0.5, 0.0)$, $S(-.5, 0.5, 0.0)$, $Y(-.5, 0.0, 0.0)$, $Z(0.0, 0.0, 0.5)$, $U(0.0, 0.5, 0.5)$, $R(-.5, 0.5, 0.5)$, $T(-.5, 0.0, 0.5)$; **(b)** spin-projected total density of states (TDOS); **(c)** partial density of states (PDOS) of $Pt(s, p, d)$ orbitals in PtN_2; and **(d)** PDOS of $N(s, p)$ orbitals in PtN_2.

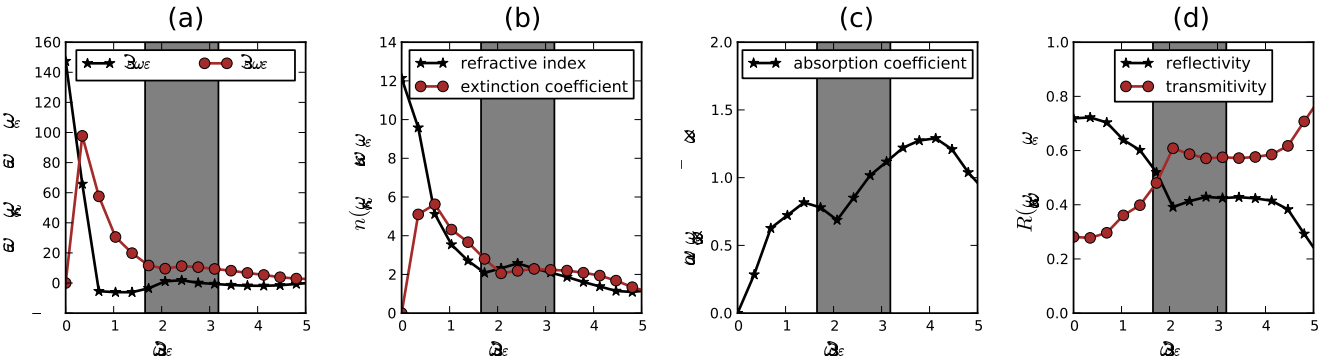

FIG. 10. (Color online.) The *GW* calculated frequency-dependent optical spectra of PtN(B3): **(a)** the real $\varepsilon_{\rm re}(\omega)$ and the imaginary $\varepsilon_{\rm im}(\omega)$ parts of the dielectric function $\varepsilon_{\rm RPA}(\omega)$; **(b)** refraction $n(\omega)$ and extinction $\kappa(\omega)$ coefficients; **(c)** absorption coefficient $\alpha(\omega)$; and **(d)** reflectivity $R(\omega)$ and transmitivity $T(\omega)$. The shaded window highlights the optical region.

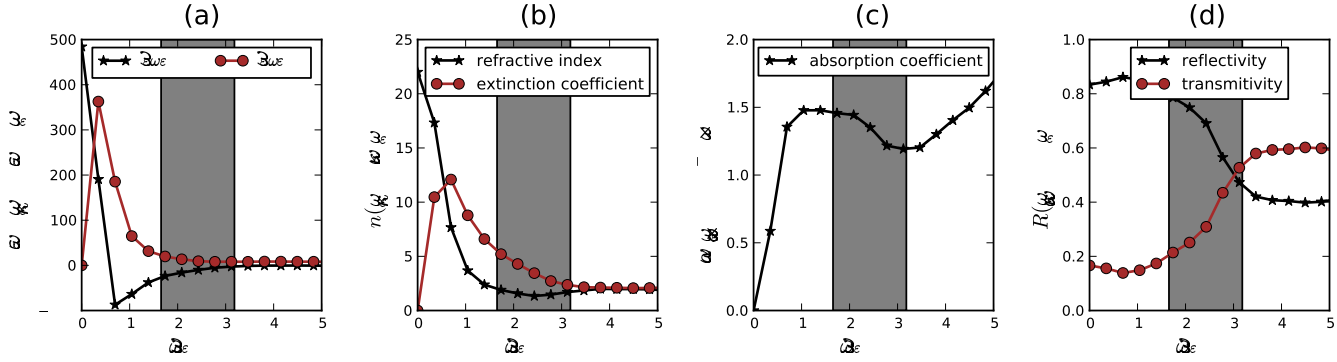

FIG. 11. (Color online.) The *GW* calculated frequency-dependent optical spectra of PtN(B17): **(a)** the real $\varepsilon_{\rm re}(\omega)$ and the imaginary $\varepsilon_{\rm im}(\omega)$ parts of the dielectric function $\varepsilon_{\rm RPA}(\omega)$; **(b)** refraction $n(\omega)$ and extinction $\kappa(\omega)$ coefficients; **(c)** absorption coefficient $\alpha(\omega)$; and **(d)** reflectivity $R(\omega)$ and transmitivity $T(\omega)$. The shaded window highlights the optical region.

poor metal[8], and we found PtN_2(C18) to be a semiconductor with a small band gap.

Hence, in contrast to the proposed PtN modifications, PtN_2 phases possess many similar properties as the synthesized phase[76].

IV. CONCLUSIONS

In summary, we presented a systematic series of first-principles calculations of the energy-optimized geometries, phase stabilities and electronic and optical properties of bulk Pt_3N, PtN and PtN_2 in twenty different crystal structures. Comprehensive comparison with experiment and with previous calculations has been made, and excellent agreement has been achieved. We found that both the lowest energy and the highest bulk modulus phases belong to the PtN_2 series and not to the PtN family. Moreover, the calculated electronic and optical properties of the PtN_2 phases show stronger consistency with experiment than the claimed PtN(B3) phase. In the present work, we have investigated a wider parameter sub-space than previous calculations, and to the best of our knowledge, the present work is the first to propose and to study the physical properties of Pt_3N, as well as the first to theoretically calculate the optical spectra of this new material. However, optical properties of PtN_2(C1 and C2) have not been investigated, and we strongly recommend optical calculations for these phases and obtained results should be tested against experiment. Moreover, experimentalists should provide the community with more data.

ACKNOWLEDGMENTS

We thank the CHPC for providing the supercomputer facilities to perform the GW calculations. Suleiman would like to acknowledge the support he received from Wits, DAAD, AIMS, SUST, and the ASESMA and the KWAMS13 groups.

* Corresponding author: suleiman@aims.ac.za
† Homepage: http://www.wits.ac.za/staff/daniel.joubert2.htm

[1] E. Gregoryanz, C. Sanloup, M. Somayazulu, J. Badro, G. Fiquet, H. kwang Mao, and R. J. Hemley, Nature Materials **3**, 294 (April 2004), http://www.nature.com/nmat/journal/v3/n5/full/nmat1115.html
[2] A. Citra, X. Wang, W. D. Bare, and L. Andrews, The Journal of Physical Chemistry A **105**, 7799 (2001), http://pubs.acs.org/doi/pdf/10.1021/jp011542l, http://pubs.acs.org/doi/abs/10.1021/jp011542l
[3] G. Soto, Materials Letters **58**, 2178 (2004), ISSN 0167-577X, http://www.sciencedirect.com/science/article/pii/S0167577X04000650
[4] J. C. Crowhurst, A. F. Goncharov, B. Sadigh, C. L. Evans, P. G. Morrall, J. L. Ferreira, and A. J. Nelson, Science **311**, 1275 (2006), http://www.sciencemag.org/content/311/5765/1275.full.pdf, http://www.sciencemag.org/content/311/5765/1275.abstract
[5] F. Chang-Zeng, S. Li-Ling, W. Yuan-Xu, W. Zun-Jie, L. Ri-Ping, Z. Song-Yan, and W. Wen-Kui, Chinese Physics Letters **22**, 2637 (2005), http://stacks.iop.org/0256-307X/22/i=10/a=050
[6] A. F. Young, J. A. Montoya, C. Sanloup, M. Lazzeri, E. Gregoryanz, and S. Scandolo, Phys. Rev. B **73**, 153102 (Apr 2006), http://link.aps.org/doi/10.1103/PhysRevB.73.153102
[7] X. Zhang, G. Trimarchi, and A. Zunger, Physical Review B **79**, 092102 (Mar 2009), http://link.aps.org/doi/10.1103/PhysRevB.79.092102
[8] R. Yu, Q. Zhan, and X. F. Zhang, Applied Physics Letters **88**, 051913 (2006), http://link.aip.org/link/?APL/88/051913/1
[9] J. von Appen, M.-W. Lumey, and R. Dronskowski, Angewandte Chemie International Edition **45**, 4365 (2006), ISSN 1521-3773, http://dx.doi.org/10.1002/anie.200600431
[10] S. K. R. Patil, S. V. Khare, B. R. Tuttle, J. K. Bording, and S. Kodambaka, Physical Review B **73**, 104118 (Mar 2006), http://link.aps.org/doi/10.1103/PhysRevB.73.104118
[11] A. F. Wells, *Structural Inorganic Chemistry*, 5th ed. (Oxford University Press, 1984)
[12] N. Brese and M. O'Keeffe, in *Complexes, Clusters and Crystal Chemistry*, Structure and Bonding, Vol. 79 (Springer Berlin Heidelberg, 1992) pp. 307–378, ISBN 978-3-540-55095-2, http://dx.doi.org/10.1007/BFb0036504
[13] M. Haisa, Acta Crystallographica Section A **38**, 443 (Jul 1982), http://dx.doi.org/10.1107/S0567739482000990
[14] G. Kresse and J. Hafner, Physical Review B **47**, 558 (Jan 1993), http://link.aps.org/doi/10.1103/PhysRevB.47.558
[15] G. Kresse and J. Hafner, Physical Review B **49**, 14251 (May 1994), http://link.aps.org/doi/10.1103/PhysRevB.49.14251
[16] G. Kresse and J. Furthmller, Computational Materials Science **6**, 15 (1996), ISSN 0927-0256, http://www.sciencedirect.com/science/article/pii/0927025696000
[17] G. Kresse and J. Furthmüller, Physical Review B **54**, 11169 (Oct 1996), http://link.aps.org/doi/10.1103/PhysRevB.54.11169
[18] J. Hafner, Journal of Computational Chemistry **29**, 2044 (2008), ISSN 1096-987X, http://dx.doi.org/10.1002/jcc.21057
[19] G. Kresse and D. P. Joubert, Physical Review B **59**, 1758 (Jan 1999), http://link.aps.org/doi/10.1103/PhysRevB.59.1758
[20] U. von Barth and L. Hedin, Journal of Physics C: Solid State Physics **5**, 1629 (Feb 1972), http://iopscience.iop.org/0022-3719/5/13/012/

[21] M. Pant and A. Rajagopal, Solid State Communications **10**, 1157 (1972), ISSN 0038-1098, http://www.sciencedirect.com/science/article/pii/0038109872900749

[22] W. Kohn and L. J. Sham, Physical Review **140**, A1133 (Nov 1965), http://link.aps.org/doi/10.1103/PhysRev.140.A1133

[23] H. J. Monkhorst and J. D. Pack, Physical Review B **13**, 5188 (Jun 1976), http://link.aps.org/doi/10.1103/PhysRevB.13.5188

[24] O. Jepson and O. Anderson, Solid State Communications **9**, 1763 (1971), ISSN 0038-1098, http://www.sciencedirect.com/science/article/pii/0038109871903139

[25] G. Lehmann and M. Taut, physica status solidi (b) **54**, 469 (1972), ISSN 1521-3951, http://dx.doi.org/10.1002/pssb.2220540211

[26] P. E. Blöchl, O. Jepsen, and O. K. Andersen, Physical Review B **49**, 16223 (Jun 1994), http://link.aps.org/doi/10.1103/PhysRevB.49.16223

[27] M. Methfessel and A. T. Paxton, Physical Review B **40**, 3616 (Aug 1989), http://link.aps.org/doi/10.1103/PhysRevB.40.3616

[28] J. P. Perdew, K. Burke, and M. Ernzerhof, Physical Review Letters **77**, 3865 (Oct 1996), http://link.aps.org/doi/10.1103/PhysRevLett.77.3865

[29] J. P. Perdew, K. Burke, and M. Ernzerhof, Physical Review Letters **78**, 1396 (Feb 1997), http://link.aps.org/doi/10.1103/PhysRevLett.78.1396

[30] M. Ernzerhof and G. E. Scuseria, The Journal of Chemical Physics **110**, 5029 (1999), http://link.aip.org/link/?JCP/110/5029/1

[31] A. D. Becke, Physical Review A **38**, 3098 (Sep 1988), http://link.aps.org/doi/10.1103/PhysRevA.38.3098

[32] J. P. Perdew, J. A. Chevary, S. H. Vosko, K. A. Jackson, M. R. Pederson, D. J. Singh, and C. Fiolhais, Physical Review B **46**, 6671 (Sep 1992), http://link.aps.org/doi/10.1103/PhysRevB.46.6671

[33] J. P. Perdew, J. A. Chevary, S. H. Vosko, K. A. Jackson, M. R. Pederson, D. J. Singh, and C. Fiolhais, Physical Review B **48**, 4978 (Aug 1993), http://link.aps.org/doi/10.1103/PhysRevB.48.4978.2

[34] P. E. Blöchl, Physical Review B **50**, 17953 (Dec 1994), http://link.aps.org/doi/10.1103/PhysRevB.50.17953

[35] E. R. Davidson, Journal of Computational Physics **17**, 87 (1975), ISSN 0021-9991, http://www.sciencedirect.com/science/article/pii/0021999175900650

[36] R. P. Feynman, Physical Review **56**, 340 (Aug 1939), http://link.aps.org/doi/10.1103/PhysRev.56.340

[37] G. Grimvall, *Thermophysical Properties of Materials* (North Holland, 1986)

[38] M. S. H. Suleiman, M. P. Molepo, and D. P. Joubert, ArXiv e-prints(Nov. 2012), arXiv:1211.0179 [cond-mat.mtrl-sci]

[39] F. Birch, Physical Review **71**, 809 (Jun 1947), http://link.aps.org/doi/10.1103/PhysRev.71.809

[40] R. W. G. Wyckoff, *The Structure of Crystals* (The Chemical Catalog Co., New York, 1935)

[41] M. D. Graef and M. E. McHenry, *Structure of materials : An Introduction to Crystallography, Diffraction and Symmetry* (Cambridge University Press, 2007) http://www.cambridge.org/9780521651516

[42] *Handbook of Mineralogy*, edited by J. W. Anthony, R. A. Bideaux, K. W. Bladh, and M. C. Nichols (Mineralogical Society of America, Chantilly, VA 20151-1110, USA) available on-line at http://www.handbookofmineralogy.org/

[43] M. S. H. Suleiman, M. P. Molepo, and D. P. Joubert, ArXiv e-prints(Nov. 2012), arXiv:1211.0179 [cond-mat.mtrl-sci], http://arxiv.org/abs/1211.0179

[44] M. Gajdoš and K. Hummer and G. Kresse and J. Furthmüller and F. Bechstedt, Physical Review B **73**, 045112 (Jan 2006), http://link.aps.org/doi/10.1103/PhysRevB.73.045112

[45] W. G. Aulbur, L. Jönsson, and J. W. Wilkins (Academic Press, 1999) pp. 1 – 218, http://www.sciencedirect.com/science/article/pii/S0081194708

[46] J. Kohanoff, *Electronic Structure Calculations for Solids and Molecules : Theory and Computational Methods* (Cambridge University Press; Cambridge, 2006)

[47] J. Harl, *The Linear Response Function in Density Functional Theory: Optical Spectra and Improved Description of the Electron Correlation*, Ph.D. thesis, University of Vienna (2008), http://othes.univie.ac.at/2622/

[48] G. Kresse, M. Marsman, and J. Furthmuller, "Vasp the guide," (2011), available on-line at http://cms.mpi.univie.ac.at/vasp/vasp/. Last accessed October 2012.

[49] M. Fox, *Optical Properties of Solids*, Oxford Master Series in Physics: Condensed Matter Physics (Oxford University Press, 2010) ISBN 9780199573363, http://books.google.co.za/books?id=-5bVBbAoaGoC

[50] M. Dressel and G. Grüner, *Electrodynamics of solids : optical properties of electrons in matter* (Cambridge University Press, Cambridge New York, 2002) ISBN 0521592534

[51] A. Miller, in *Handbook of Optics, Volume 1: Fundamentals, Techniques Optical Society of America* (McGraw-Hill, Inc., New York, NY, USA, 2010) ISBN 0070479747, 9780070479746

[52] M. Rohlfing and S. G. Louie, Physical Review B **62**, 4927 (Aug 2000), http://link.aps.org/doi/10.1103/PhysRevB.62.4927

[53] J. Donohue, *The structures of the elements*, A Wiley-interscience publication (John Wiley & Sons Inc., 1974) ISBN 0471217883, http://books.google.co.za/books?id=Q-rvAAAAMAAJ

[54] C. Kittel, *Introduction to Solid State Physics*, eigth ed. (John Wiley & Sons, Inc., 2005) ISBN 9780471415268, http://books.google.co.za/books?id=kym4QgAACAAJ

[55] S. Raju, E. Mohandas, and V. Raghunathan, J. Phys. Chem Solids **58**, 1367 (1997)

[56] M. J. Mehl and D. A. Papaconstantopoulos, Physical Review B **54**, 4519 (Aug 1996), http://link.aps.org/doi/10.1103/PhysRevB.54.4519

[57] E. Zarechnaya, N. Skorodumova, S. Simak, B. Johansson, and E. Isaev, Computational Materials Science **43**, 522 (2008), ISSN 0927-0256, http://www.sciencedirect.com/science/article/pii/S0927025608

[58] A. Dewaele, P. Loubeyre, and M. Mezouar, Phys. Rev. B **70**, 094112 (Sep 2004), http://link.aps.org/doi/10.1103/PhysRevB.70.094112

[59] L. Yu, K. Yao, Z. Liu, and Y. Zhang, Physica B: Condensed Matter **399**, 50 (2007), ISSN 0921-4526, http://www.sciencedirect.com/science/article/pii/S0921452607

[60] W. Chen, J. Tse, and J. Jiang, Solid State Communications **150**, 181 (2010), ISSN 0038-1098, http://www.sciencedirect.com/science/article/pii/S0038109809

[61] M. S. H. Suleiman and D. P. Joubert, ArXiv e-prints(Dec. 2012), arXiv:1212.6507 [cond-mat.mtrl-sci],

http://arxiv.org/abs/1212.6507
[62] M. S. H. Suleiman and D. P. Joubert, in *South African Institute of Physics 57th Annual Conference (SAIP 2012), No. 298* (2012) http://indico.saip.org.za/confSpeakerIndex.py?view=full&letterBookOfId=14
[63] M. S. H. Suleiman and D. P. Joubert, in *South African Institute of Physics 57th Annual Conference (SAIP 2012), No. 299* (2012) http://indico.saip.org.za/confSpeakerIndex.py?view=full&letter=s&confId=14
[64] L. J. Cabri, J. H. G. Laflamme, J. M. Stewart, K. Turner, and B. J. Skinner, American Mineralogist **63**, 832 (1978), http://www.minsocam.org/msa/collectors_corner/amtoc/toc1978.htm
[65] Surprisingly, Chen, Tse and Jiang[60] got exactly the same V_0 values for C2 and C18 within both GGA and LDA; but the average values they gave are different! Thus, we suspect the equal V_0 values they gave for C2 and C18 in both GGA and LDA (see Table 1 in that article); and it may be a typo.
[66] These are $H(P)$ diagrams but relative to their elemental constituents.
[67] M. S. H. Suleiman and D. P. Joubert, ArXiv e-prints(Dec. 2012), arXiv:1212.6507 [cond-mat.mtrl-sci]
[68] Recall that we only consider values relative to Pt(A1) to eliminate systematic errors.
[69] R. Yu, Q. Zhan, and X. F. Zhang, Applied Physics Letters **88**, 051913 (2006), http://link.aip.org/link/?APL/88/051913/1
[70] Fixing the lattice parameter at the experimental value $a = 4.8041$ Å, Ref. 6 relaxed the N ions and obtained the same value $u = 0.415$.
[71] C. J. Bradley and A. P. Cracknell, *The Mathematical Theory of Symmetry in Solids: Representation Theory for Point Groups and Space Groups* (Oxford: Clarendon Press, 1972)
[72] Z. Wu and R. E. Cohen, Physical Review B **73**, 235116 (Jun 2006), http://link.aps.org/doi/10.1103/PhysRevB.73.235116
[73] V. N. Staroverov, G. E. Scuseria, J. Tao, and J. P. Perdew, Physical Review B **69**, 075102 (Feb 2004), http://link.aps.org/doi/10.1103/PhysRevB.69.075102
[74] J. P. Perdew and S. Kurth, in *A Primer in Density Functional Theory*, Lecture Notes in Physics (Springer, 2003) ISBN 9783540030836, http://books.google.co.za/books?id=mX793GABep8C
[75] J. C. Grossman, A. Mizel, M. Côté, M. L. Cohen, and S. G. Louie, Physical Review B **60**, 6343 (Sep 1999), http://link.aps.org/doi/10.1103/PhysRevB.60.6343
[76] Such an observation was arrived at by other authors[8] for the PtN(C1). Here we are making more comprehensive comparison